Progress Report On Contract # N00014-99-C-0415

"pT Spin Dependent Tunneling Sensor"

Submitted To: Dr. Larry Cooper, Office of Naval Research

Principal Investigator: James M. Daughton
Contributors: Cathy Nordman, Dave Brownell, Dan Reed
Nonvolatile Electronics, Inc. (NVE)
11409 Valley View Road
Eden Prairie, MN 55344
Phone: (612) 996-1607
Fax: (612) 996-1600

Contract Amount: $200,000
Duration: 9 Months
Period of Performance: August 30, 1999 to May 31, 2000

Submitted: September 30, 1999

PROGRAM SUMMARY

The purpose of this program is to develop magnetic field sensors using Spin Dependent Tunneling (SDT) material for use in low field applications (1-100 pT). Presently, low field applications typically require fluxgate magnetometers or SQUID magnetometers. Spin Dependent Tunneling (SDT) devices offer an order of magnitude improvement in low field sensing over Giant Magnetoresistance (GMR) sensors due to their intrinsically higher magnetoresistance (20%-40%) and relatively small saturation fields (2 Oe – 10 Oe). In addition, higher resistance values are relatively easy to attain in small areas, making it possible to have miniaturized devices with low power consumption. The SDT sensors developed under this contract should be very small (SOIC-8 package), should require little power, and should be easily combined with other electronics. If the program is successful, the SDT sensors should have distinct advantages in both commercial and military applications.

The most significant sensor operating parameters are resolution, frequency range, and power consumption. This program has the objective of demonstrating a SDT bridge sensor with the following properties:

- 1 pT / $\sqrt{Hz}$ noise floor @ 1 Hz
- Sensor optimization for use in the 1 to 300 Hz frequency range
- A zero-power field biased linear operating mode

The program has been divided into seven tasks: 1) Program Plan, 2) SDT Materials Improvements, 3) Low Frequency Circuitry, 4) Low Power Biasing, 5) Complete Sensor Assembly, 6) Final Report, and 7) Program Management as shown in the following chart (with a planned start date of July 1, 1999):

PROGRAM SCHEDULE
Spin Dependent Tunneling Sensors for Low Frequency - Low Field - Low Power Applications

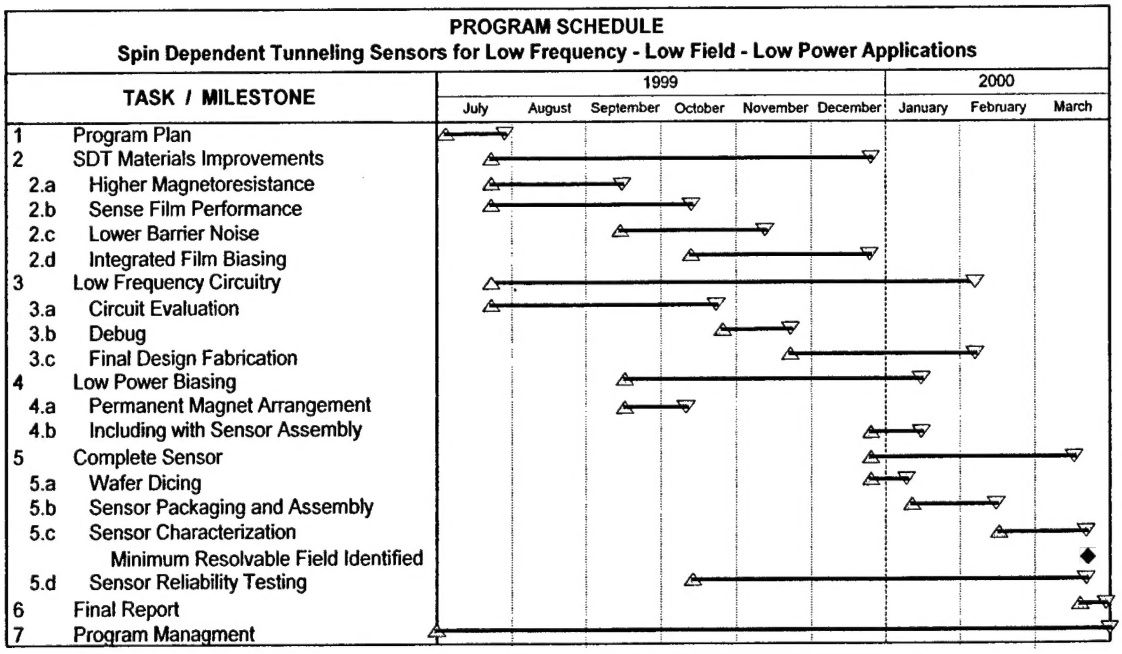

DISTRIBUTION STATEMENT AUTHORIZATION RECORD

Title: PT Spin Dependent Tunneling Sensor

Authorizing Official: Dr. Larry Cooper

Agency: ONR Ph. No. (703) 696-4215

☐ Internet Document: URL: _____
(DTIC-OCA Use Only)

Distribution Statement: (Authorized by the source above.)

☒ **A:** Approved for public release, distribution unlimited.

☐ **B:** U. S. Government agencies only. (Fill in reason and date applied). Other requests shall be referred to (Insert controlling office).

☐ **C:** U. S. Government agencies and their contractors. (Fill in reason and date applied). Other requests shall be referred to (Insert controlling office).

☐ **D:** DoD and DoD contractors only. (Fill in reason and date applied). Other requests shall be referred to (Insert controlling office).

☐ **E:** DoD components only. (Fill in reason and date applied). Other requests shall be referred to (Insert controlling office).

☐ **F:** Further dissemination only as directed by (Insert controlling DoD office and date), or higher authority.

☐ **X:** U. S. Government agencies and private individuals or enterprises eligible to obtain export-controlled technical data in accordance with DoD Directive 5230.25.

NOTES: Missing distribution statement

J. Keith
DTIC Point of Contact

16 Nov 99
Date

The first part of the program is devoted to material improvements and to evaluation of circuits to reduce the effects of 1/f noise.

In the first month of the program substantial progress was made in several areas. First, sensor and corresponding mask designs have been completed which should result in both lower noise and higher sensitivity compared to previous designs. Second, junctions have been produced on thick (~1000A) copper substrates, which should lower noise. Third, noise in SDT junctions has been characterized, with most of the 1/f noise being non-magnetic, i.e. the noise doesn't change appreciably when a strong magnetic is brought near the junction. However, the 1/f noise behaves like a resistor change, and normal voltage chopping doesn't get rid of the noise. We are currently evaluating schemes whereby varying the sensitivity using bias magnetic fields should allow significant separation of the 1/f noise from the magnetic signal.

The remainder of this report is divided into four sections. The first is a description of the design concept updated for latest findings (Jim Daughton). The second section describes the sensor design and mask set which will be used for this program (Cathy Nordman). The third summarizes the progress in processing, particularly adding a copper layer under the junction (Dave Brownell). The fourth summarizes noise status (Dan Reed).

Part 1 - Low Field SDT Sensor Design Considerations – Jim Daughton

A. Previous Design – In our previous sensor designs the effects of non-uniform demagnetizing/stray fields reduced sensitivity of biased SDT sensing elements and introduced considerable hysteresis. This section analyzes the reasons for this effect and outlines the basis for new designs.

The basic configuration of the bias and easy direction of the SDT sensor is shown below:

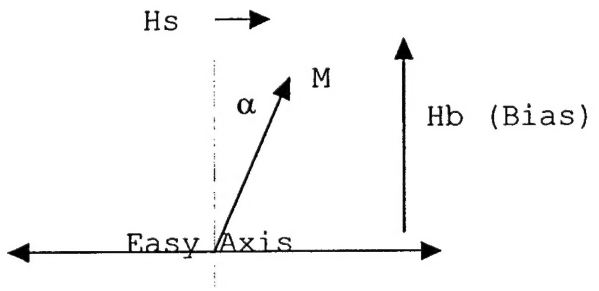

The bias Hb is intended to be slightly higher than Hk, and if the torque equation is written in terms of α, the angle the magnetization makes with respect to the bias field, then

$$Hs*Cos\alpha - Hb*Sin\alpha + Hk*Sin\alpha Cos\alpha = 0$$

Now let Hb = Hk$(1 + \delta)$, and let Hs/Hk = hs. Then,

$$hs*Cos\,\alpha - Sin\alpha[1 + \delta - Cos\,\alpha] = 0, \text{ or}$$

$$hs = Sin\alpha[1 + \delta - Cos\,\alpha]/Cos\,\alpha$$

Let α and δ be small, then

$$hs = \alpha\delta, \text{ or } \alpha = hs/\delta$$

Now since the effective resistance varies as Sinα,

$$(\Delta R/R)(100\%) = (JMR/2)Sin\alpha \sim (JMR/2)\alpha = (JMR/2)hs/\delta$$

This is the ideal expression for the operation of the sensor. For example, if Hk = 15 Oe, JMR = 20%, and δ = 1.5 Oe, then the ratio ΔR/Hs would be about 7%/Oe, a respectable sensitivity. This mathematical model would suggest that an infinite sensitivity as δ approaches zero. Because of non-ideal behavior of the magnetic film, an infinite sensitivity would not be possible. Two non-ideal characteristics will now be discussed: angular dispersion and anisotropy dispersion. Angular dispersion of the easy axis is typically from about 0.5 degrees to about 2 degrees in "good" uniaxial magnetic films. This is interpreted

as meaning that the local easy axes in roughly 90% of the film is within plus or minus the stated values. Anisotropy constant dispersion (or Hk dispersion) is difficult to measure, and is really probably very small (a few percent). However, a non-uniform bias field can have the same kinds of effects as Hk dispersion, and can be much larger in equivalence unless care is taken to make it small.

The effects of angular dispersion can be viewed by considering a number of small regions in the film with various easy axes. If the easy axis of a region lies at an angle to the intended easy axis making an angle α_0 with it, then the effect on ΔR for that region can be compared to the ideal case. Then

$$Hs*Cos\alpha - Hb*Sin\alpha + Hk*Sin(\alpha - \alpha_0)Cos(\alpha - \alpha_0)= 0$$

Now, as before, let $Hb = Hk(1 + \delta)$, and let $Hs/Hk = hs$. Then

$$hsCos\alpha - (1 + \delta)Sin\alpha + Sin(\alpha - \alpha_0)Cos(\alpha - \alpha_0) = 0$$

Assuming both α and α_0 are small, and δ is small,

$$Sin(\alpha - \alpha_0)Cos(\alpha - \alpha_0) \sim (\alpha - \alpha_0) \text{ and}$$

$$hs = \delta\alpha - \alpha_0 \text{, or } \alpha = (hs + \alpha_0)/ \delta \text{ .}$$

This simply represents an offset (with no field applied) of α_0/ δ, but the change of angle (and hence sensitivity) is unchanged. This could be a very significant offset compared to the signal levels, but can be calibrated out in a sensor. The angular dispersion would be a problem if the dispersion were large enough that the signal would be present outside the high sensitivity region near $\alpha = 0$. That is not as likely, however, as the nonuniformity of demagnetizing fields cause more serious problems.

Suppose the bias field varies, (or there is high anisotropy dispersion, which is equivalent). As in the angular dispersion study, the sensor can be considered as a collection of small areas with varying properties. If the bias field is much higher than Hk, the previous analysis is still valid. The effect of higher Hk values is then to increase δ and to decrease sensitivity by the factor $1/\delta$. With high biases, the output would still be linear and there would be no hysteresis. A worse effect happens when the bias is slightly lower than Hk. There are two stable states possible when the bias is below Hk, and as the field Hs is varied through switching points, the magnetization will switch from one stable state to the other, creating hysteresis in the resistance of the device. If δ is small but negative, and if α is small, the extent of the hysteresis can be determined by the relationship

$$cos\alpha \sim 1 - \alpha^2/2.$$

Then plugging into the case where hs = 0, and assuming α is not 0 (which it isn't), one gets

$$-\delta \sim \alpha^2/2, \text{ or } \alpha = +/-\text{sq rt}(-2\delta).$$

Suppose δ = -0.1, then α would be +/-sq rt (0.2) or +/-0.447 (about +/-25 degrees). This would be a very high hysteresis. The switch point would be given from the expression

$$hs^{2/3} + (1 + \delta)^{2/3} = 1.$$

For the above example, hs would reach a switch point at about 0.017. For a value of Hk of 15 Oe, this would be a magnetic field of 0.26 Oe. The sensitivity would be about as for δ = + 0.1, but the practicality of such a mode of operation would be questionable. The sensor could be operated with a value of δ much more negative, and the switching fields would increase. However, the sensitivity would decrease as well, and there would still be two stable states, only with higher values of switching fields. It is clear that operating with a bias slightly under Hk is not a good idea, and it is also likely that operating with a bias well under Hk gives low sensitivity, and still has potential instabilities, albeit at higher fields.

Thus, the tentative conclusion is that bias in the SDT sensor should be kept above Hk over nearly all of the active area of the sensor. Next the current design will be assessed to see how well this condition can be met.

The essence of the unit SDT cells is a pair of hard magnetic contact areas (pinned in the easy direction of the soft layer) and a single soft layer (which is biased in the hard direction). There are two junctions in series, with the soft layer acting also as a series connection between the junctions.

Neighboring elements in a close-packed array could reduce demagnetizing fields and improve uniformity. But for the purposes of this analysis, the neighbors are ignored.

The most elemental shape of the soft layer is a rectangle with the active area pulled in by 2 microns all round. The actual shapes (football or pointed end shapes) should be somewhat better. Ideally, the demagnetizing fields would behave like an inscribed ellipsoid for fields less than the fields necessary to saturate the layer.

Consider the following case for non-uniformity, which would be worst case. If enough bias is applied to saturate the soft layer, one could consider line charges at each end of the cell. If the soft layer is 22 microns x 38 microns, approximate this with a 30 micron x 30 micron rectangle with an inscribed 26 micron x 26 micron active area. To a very crude approximation, the field 2 microns from the end would be (12,000 Gauss)(film thickness microns)/2π*2 microns. If the film thickness is 125 A (12.5 x 10^{-3} micron), at 2 microns, the demagnetizing field would be 11.9 Oe. At 26 microns, the field would be (2/26)*11.9 = 0.9 Oe. At each end the field would be 12.8 Oe. In the center, the field would be 2*(2/13)*11.9 = 3.7 Oe. Thus there would be a variation of fields

over the active area from 12.8 Oe down to 3.7 Oe. With an Hk of 15 Oe, at least 27.8 Oe would have to be applied to saturate the ends, which would make the ends sensitive, but the center would have an δ of 9.1 Oe, making the center relatively insensitve to applied fields.

An elliptical shape would help this non-uniform field condition, but not necessarily do away with it. The current design allows only 2 micron spacing from the end of the soft layer to the active layer. The requirement to saturate to the end of the active layer will necessarily mean a very non-uniform demagnetizing field in the active layer so long as the active area is only 2 microns from the end of the cell.

Another demagnetizing consideration also causes difficulties with sensitivity. The easy direction demagnetizing field (Hd) for an inscribed ellipsoid of 20 micron diameter is approximately

$$0.785*12{,}500*(12.5 \times 10^{-3})/20 = 6 \text{ Oe.}$$

This adds a term to the torque equation which effectively reduces the sensitivity. A torque term of $Hd*\cos\alpha*\sin\alpha$ acts to reduce the effective Hk. If this demagnetizing field is non-uniform, then the effect is like an anisotropy dispersion. Also, the way the devices are currently arranged, there is a very non-uniform field in the easy direction due to the pinned layer. At the edges of the pinned layer, this will bias the device on the order of several Oe, even for thin pinning layers.

From the foregoing, it seems necessary to:

1) Make the soft layer as thin as possible, while still providing for a good series connection between SDT devices through the layer. This could be done with a thin underlayer of non-magnetic conducting material. A magnetic film thickness of 30-50 A could be a good target, and that would eliminate much (2/3) of the demagnetizing fields and nonuniformities in demagnetizing field. It would also help to make the whole structure larger.

2) Pull the active layer further away from the ends of the soft layer. Going from 2 microns to 4 or 5 would help. Particularly pull further back from the ends in the direction of bias field.

3) Use a CoRuCo(A/F) as a pinning layer, making the two Co layers nearly the same thickness. This, too, will lower the magnitude and nonuniformity of the easy direction bias from the hard film on the soft film.

4) Because a low field change must be detected in the presence of a field as large as the earth's magnetic field, a current feedback detection scheme is highly desirable. This also provides the mechanism to keep the sensor bias in its most sensitive operate point.

New Sensor Design - For new designs, we have to make low dispersion films, and the preferred pinned layer will be a CoRuCo sandwich with low stray fields. Thus, the remaining problems are the demagnetizing fields of the soft

layer. If the layer is 100 A thick with a Ms of 10^4 Gauss, then the inscribed ellipsoid model would indicate roughly $[0.85*10^{-2}/d]*10^4$ Oe demagnetizing field, where d is the diameter of the ellipse in microns. Thus, a diameter of about 85 microns would be needed to get the demagnetizing field down to one Oe. 170 microns would be even better, but the size of the sensor might grow out of bounds.

The spacing s from the edge of the soft layer to the edge of the pinned layer should be such that the difference between the field at the edge and the field at the center is smaller than one Oe. A worst case calculation would be using line charges. Assuming saturation, the line charge would have a linear density of MsTf, where Ms is the saturation magnetization of the film and Tf is the film thickness. In this case, 10^2 Oe/micron would be the linear magnetic charge density. The stray field from this line charge would be $MsTf/2\pi s$ or 16/s Oe, where s is in microns. Note that this formula would indicate 0.67 Oe at the center of a 85 micron ellipsoid, but it's pretty well understood that the line charge model underestimates fields in the center of the body and over estimates fields near the edges, so that's OK. 16 microns would be a safe border. The overall dimensions should be about as shown below.

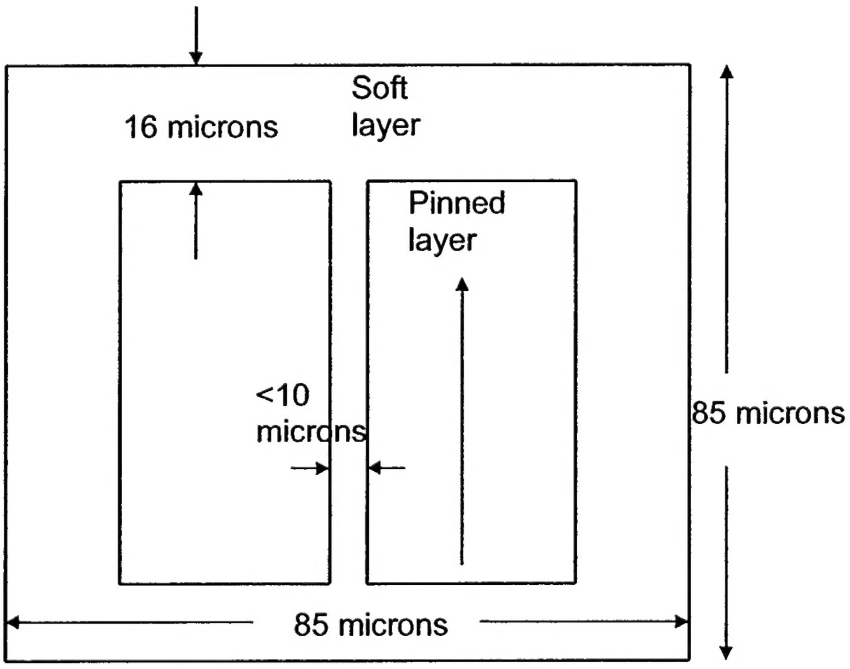

Fig. 1.1. More Uniform Magnetic Field SDT Structure

Thus the overall size is 85 microns on a side, and the active area (assuming a 10 micron gap between junctions) is 21.5 x 53 micron squared per junction. Assuming a 114KOhm-micron squared rap (resistance area product),

the resistance per junction would be 100 Ohms, or 200 Ohms for the pair of junctions. Assuming an operating voltage of 10 Volts for a bridge requires 50 junctions per leg to keep the voltage drop per junction to 100 mV, or 25 of the pairs of junctions shown above. Adding 10 microns to each edge for a border, the pair of junctions would occupy 95x95 microns, or about 10^4 microns squared, and the bridge would occupy an area of 100 x 10^4 microns squared (about 1000 microns on a side or 40 mils on a side).

With excellent low dispersion films, the sensitivity of the bridge could be about 10%/Oe. The resistance of the bridge would be 5KOhms for this example. If the rap could be reduced to 20Kohm-micron squared, then the resistance would be about 500 Ohms, and the Johnson noise would be low enough to make reaching the pT/rt Hz goal feasible.

Part 2 – Low Field Sensor Reticle Set – Cathy Nordman

General overview - The reticle set designed for this program (as shown in Fig. 2.1) is intended for the investigation and improvement of NVE's spin-dependent tunneling (SDT) sensors in the areas of soft layer magnetic uniformity, sensitivity, signal to noise ratio, magnetic bias efficiency, and power consumption. The designs include 2 junction types, accommodations for 2 fabrication methods, 4 different modes of sensor operation, and a total of 8 design variations. Each of the prototype die are designed to fit standard SOIC 8-pin packages, and have bond pad features suitable for hybrid packaging with other sensor die or a chip with conditioning electronics.

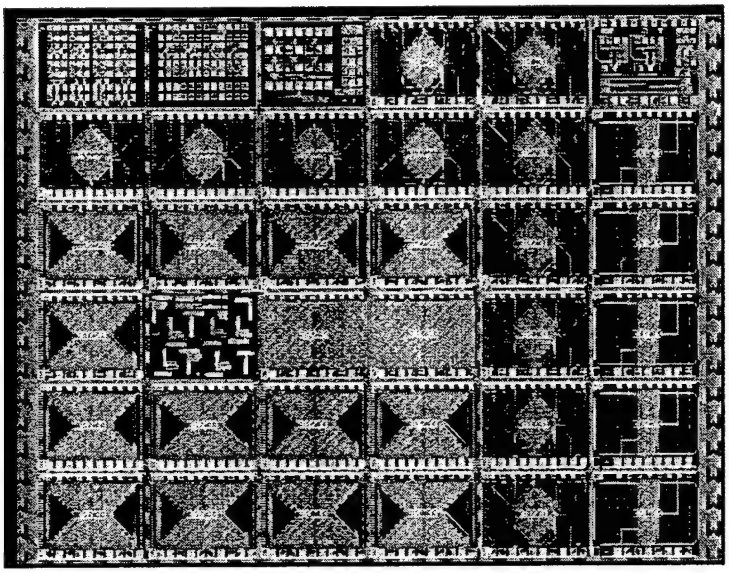

Fig. 2.1. ICED layout of the full reticle showing 8 different variations of spin-dependent-tunneling device designs.

Tunnel Junction Design - On the reticle set there are 2 geometrical designs for the tunnel junctions. One is a modification and improvement of the largest design which was used on NVE's previous SDT reticle. This design will be referred to as MOD150 (it is a modified version of the junction used in NVE's die #30,150). The other is a junction design suggested by J. Daughton. (It is named JD in the ICED library and will be referred to here as NJD for "new junction design".) This newest design will improve the stray magnetic fields and demagnetizing magnetic field uniformity over the junction area.

The layout dimensions of the NJD are shown in Fig. 2.3 below. The standard fabrication design for all of NVE's SDT resistors (the legs that form a Wheatstone bridge) are a series connection of SDT junction elements. Each element consists of two tunnel junctions which are connected by a common bottom electode (see Fig. 2.2). Metal interconnects are used on the top to connect each (double) junction element in series.

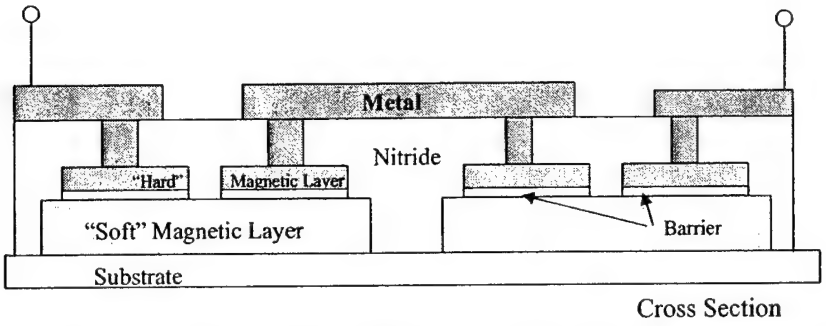

Fig. 2. 2. Cross section figure of 2 SDT junction elements (4 SDT junctions) connected in series.

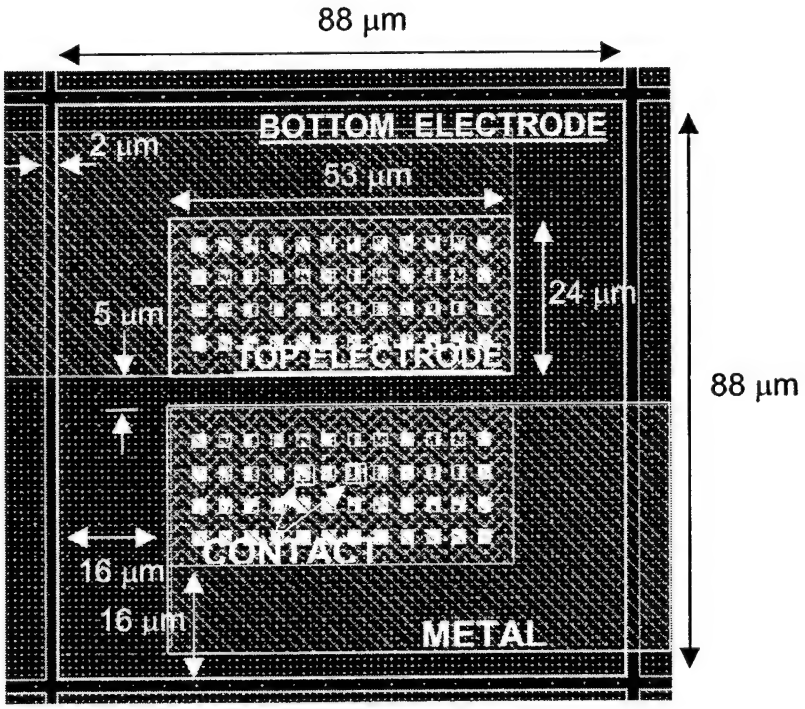

Fig. 2.3. ICED drawing of the NJD element. In-plane dimensions for the top and bottom magnetic layers are shown. "Lower Electrode" refers to the lower, soft, magnetic film, and "Top Electrode" refers to the pinned or hard magnetic layer. Separation between the soft layers of adjacent NJD elements are 2 microns.

The intention of the inplane dimensions of the large bottom electrode are to lower the demagnetizing fields of the soft layer. The top magnetic film is also pulled away from the edge of the bottom film in order to position the junction over an area of the soft film which is not affected by non-uniformities due to edge demagnetization.

Other issues which seriously compromise junction performance include stray fields from the pinned layer, and coupling between the top and bottom magnetic layers. Both of these issues will be addressed not with the layout design, but with the materials deposition of the films comprising the junctions. It is the intention of this program to reduce the orange peel coupling across the junction by investigating chemical mechanical polishing of previously deposited underlying films, or improving the as-deposited smoothness of the films. The issue of stray fields due the edge demagnetization of the pinned layer is to be alleviated by developing a synthetic antiferromagnetic sandwich of CoRuCo.

The second junction design, MOD150, is shown in Fig. 2.4 below. The design was made to decrease the edge demagnetization effects of the soft layer in a similar fashion to the NJD, but is restricted by some of the original dimensions of the device. This particular Wheatstone bridge device includes flux concentrators and magnetic shielding of two resistor legs in the device. The improved junction design is meant to fit the rest of the original dimensions of the previous device layout.

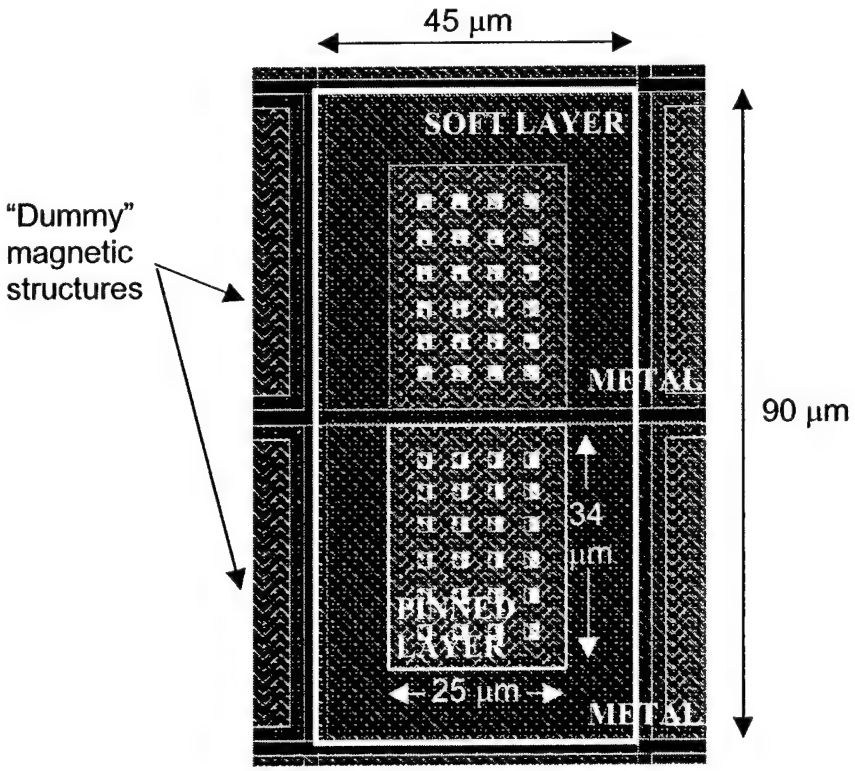

Fig. 2.4. ICED layout of MOD150 which shows the 2 magnetic layers, the metal interconnects (outlined by dashed lines) and the window contacts to the upper electrode. (See also Figs. 2 and 3.)

Estimates of Sensitivity and Noise - There are six designs with differing numbers and types of junctions and therefore differing fundamental limits on sensitivity and noise.

- One design (NVE die numbers 30226 and 30231) has 24 junctions per bridge leg, tolerates a bias voltage maximum of 4.8V (after approximately 100 mV per junction, the sensitivity decreases), and would detect a theoretical minimum field of 1.3 pT/√Hz if the assumptions are made that the final device sensitivity is 10%/Oe, the resistance-area-product of the junction is 100 KΩμm-cm^2, and the noise is the theoretical limit of Johnson noise for the resulting resistance of the bridge.
- A second 2-chip design (#30227) has 56 junctions per bridge leg, tolerates a bias voltage maximum of 11.2 V (for reasons described above), and would detect a theoretical minimum field of 1.3 pT/√Hz if the same assumptions are used.
- A third design (#s 30228, 30233) has 78 junctions per bridge leg, tolerates a bias voltage maximum of 15.6 V, and would detect a theoretical minimum field of 0.7 pT/√Hz with the same assumptions.
- Design #30229, a 2-chip device, has 156 junctions per bridge leg, tolerates a bias voltage maximum of 31.2 V, and would detect a theoretical minimum field of 0.5 pT/√Hz.
- Design #30232 also a 2-chip device, has 308 junctions per bridge leg, tolerates a bias voltage maximum of 61.2 V, and would detect a theoretical minimum field of 0.4 pT/√Hz.
- The device design with MOD150 has 12 junctions per leg, a bias voltage of 2.4 V and a theoretical minimum detectable field of 2.0 pT/√Hz

Description of Device Types - A short description of the different device types found on this reticle are given below. They are labeled by their corresponding NVE die number.

30226 Spin-dependent-tunneling (SDT) bridge sensor. Planar coil design in which 2 overlayed coils are fabricated on the chip which can produce magnetic fields in the sensing direction and a direction orthogonal to it. The device has 28 junctions per leg. The junction area is 53 x 21.5 = 1140 microns-squared. There is a 5-contact bridge option. (A laser trim site is included such that one bridge connection can be opened and therefore each leg of the bridge individually accessed. This is included in a few of the designs for test purposes.)

30227 SDT "half bridge". The bridge is actually formed by wire bonding two chips together. One chip is physically turned such that the easy direction of each chip is antiparallel. Planar coil design. 2 resistors. 56 junctions per resistor. Junction area = 53 x 21.5 = 1140 microns-squared.

30228 DT bridge sensor. Out-of-plane coil design. (The coil for producing a field in the sensing direction is formed out of the plane by using a buried metal layer below the junctions for one half of each winding, and the return path for each winding is

formed in a metal layer above the junctions.) 78 junctions per leg. Junction area = 53 x 21.5 = 1140 microns-squared. 5-contact bridge option.

30229 SDT "half bridge". Out-of-plane coil design. 2 resistors. 156 junctions per resistor. Junction area = 53 x 21.5 = 1140 microns-squared.

30230 SDT bridge sensor. Modified 30,150. Uses flux concentrators. 12 junctions per leg. Junction area = 25 x 34 = 850 microns-squared.

30231 Same as 30226 but no option for 5 contacts.

30232 SDT "half bridge". No coils. 2 resistors. 308 junctions per resistor. Junction area = 53 x 21.5 = 1140 microns-squared.

30233 Same as 30228 but no option for 5 contacts.

Device Operation and On-Chip Coils - The designs on this new reticle include options for testing and using on-chip coils for producing biasing magnetic fields in both the sensing direction and the orthogonal direction. The standard, in-plane, coils (depicted in Fig. 5) represent a preliminary option for testing the devices. Similar on-chip coils have been successfully fabricated by NVE. They do not represent an ultimate low-power solution for the devices.

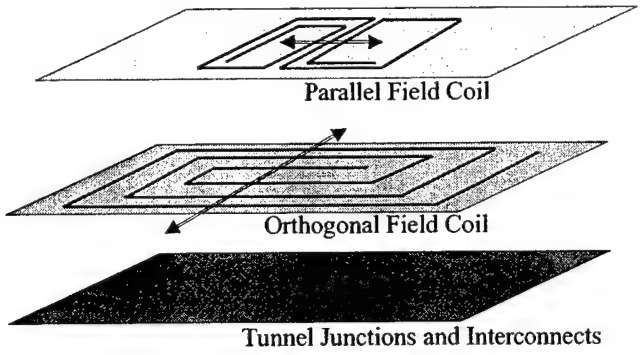

Fig. 2.5. A drawing of NVE's "standard" in-plane coils. Each coil is a subsequent layer above the tunnel junctions.

The second type of coils are depicted in Fig. 2.6 and are an experimental improvement for on-chip coils. The coil windings can be thicker because of the use of CMP in order to smooth subsequent layers, and the current efficiency of the field produced is doubled due to the windings both under and over the device, and the power efficiency is improved by more than a factor of four. The coils represent a significantly lower power option to the planar on-chip coils.

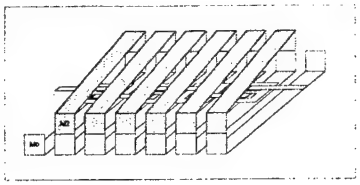

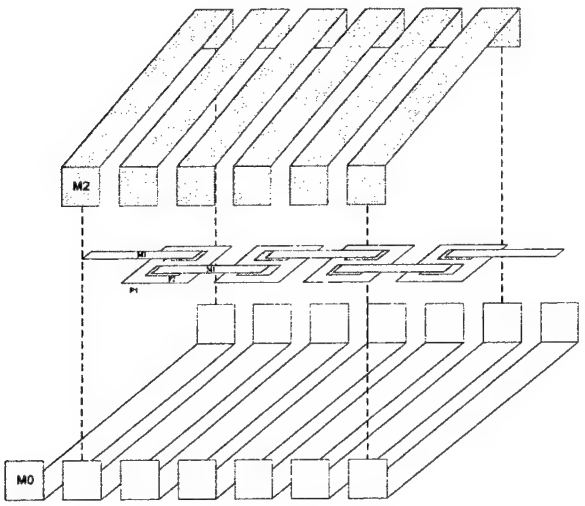

Fig. 2.6. A drawing of the out-of-plane coils that are an option on several of the SDT devices on this reticle.

The final (lowest power) option available on all of the devices is to use no on-chip coils. Other methods would be employed to reduce the need for a field in the sensing direction by externally limiting background fields and reducing any intrinsic offset due to magnetic coupling. Eliminating the orthogonal magnetic field could be achieved by permanent magnet biasing or other similar thin-film solutions.

Part 3 – SDT Sensor Process Development – Dave Brownell

The most important process development accomplishment during this period was the demonstration of functional SDT devices on CMP copper substrates. First, a number of other process runs were made to prepare for the copper substrates.

A number of lots were run which showed the capability of running ex-situ free (soft) layer deposition using 2 separate deposition systems to sputter the SDT structure. This was done to overcome the limitation of the number of targets in one system. The first lot, 93578, explored depositing the free layer in a separate sputter system. First, standard SDT wafers were deposited in-situ. The first interface variation was to deposit the free layer 30A thicker than normal and then to backsputter 30A off in the second system prior to depositing the tunnel barrier. The second approach was the same as the first, but with a 10A NiFeCo layer after back sputter to improve the interface between the free layer and the tunnel barrier. The last approach was to deposit the standard free layer thickness and add the barrier with no back sputter in the second system. In all experiments we transferred wafers directly from one system loadlock to the second systems loadlock to minimize exposure to airborne contaminants. The experimental layout and the %GMR results are shown in Table 1. Note that 2 wafers were deposited at each condition. This experiment demonstrated that we can successfully manage the ex-situ deposition of the free layer .

Table 3.1 Ex-situ Free Layer Deposition (lot 93578)

Run #	Sputter System 2400-2	Sputter System 2400-2	%GMR
1		NiFeCo 125-Al12-AlOx-CoFe50-IrMn100-Al360	9.49
2	Ta30-NiFeCo155	BS30-Al12-AlOx-CoFe50-IrMn100-Al360	11.43, 16.42
3	Ta30-NiFeCo155	BS30-NiFeCo10-Al12-AlOx-CoFe50-IrMn100-Al360	16.62, 11.52
4	Ta30-NiFeCo125	Al12-AlOx-CoFe50-IrMn100-Al360	10.91, 7.46

The second experiment was designed to investigate the copper/tunnel junction interface which would be an ex-situ interface post copper CMP. The second and third conditions used an in-situ Cu/Ta interface with varying thickness of Ta to determine the necessary thickness to prevent interdiffusion and to provide a phase break. The last condition consisted of depositing copper and exposing the copper to the slurry and clean processes used in CMP. These wafers were then backsputtered and the Ta-NiFeCo phase break and free layers were deposited. Probing the copper underlayer wafers turned out to be a challenge as the probes easily penetrate through the barrier and were seen to remove the copper from the SiN starting material. The data in Table 2 shows the

maximum %GMR values for all wafers based on 5 measurements per wafer. Run 4 of this experiment demonstrates a feasible process for depositing on CMP copper. In addition, since 10A of Ta shows good GMR results we should have good process margin at 30A copper.

Table 3.2. Ex-Situ Copper Interface Deposition

Run #	Sputter System 2400-2	Sputter System 2400-2	%GMR
1		NiFeCo 125-Al12-AlOx-CoFe50-IrMn100-Al360	7.41
2	Cu100-Ta30-NiFeCo155	BS30-Al12-AlOx-CoFe50-IrMn100-Al360	23.9,22.3
3	Cu100-Ta10-NiFeCo155	BS30-NiFeCo10-Al12-AlOx-CoFe50-IrMn100-Al360	28.9, 27.6
4	Cu Exposure BS30-Ta30-NiFeCo125	BS30-NiFeCo10-Al12-AlOx-CoFe50-IrMn100-Al360	6.3,26.6

The surface roughness of the as deposited films was characterized and as expected the roughness increased with increasing thickness. Figure 1 shows the surface roughness as a function of the as deposited film thickness. We have been able to demonstrate CMP surface roughness with an Ra of 1.8 on 750A thick films and 5.66A on 1250A thick films. CMP repeatability has shown to be a difficult task since the consumables change with time which changes the polishing process and surface roughness. The polishing pad and the carrier pad that is behind the wafer both degrade with time. A major step in polishing control was getting the chiller in place and controlling the polishing pad surface temperature. In addition, we have also learned that the amount of polishing pad rinsing between wafers seems to play a major role in consistency.

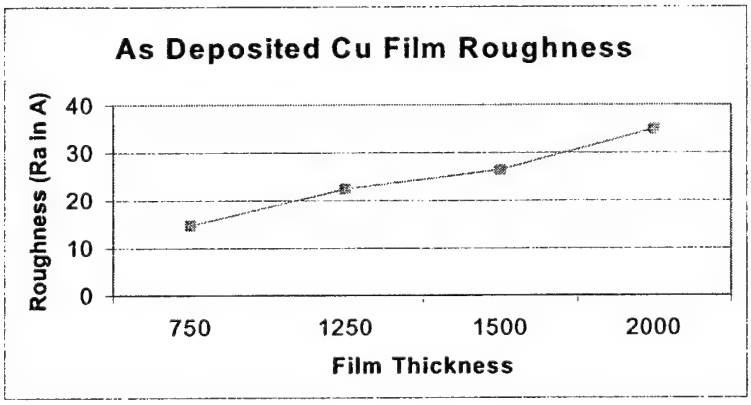

Fig. 3.1. As Deposited Surface Roughness

A third experiment used ex-situ deposition on CMP copper films of varying surface roughness. In order to build this structure, wafers with a 100A Ta adhesion layer followed by two different thickness of copper were polished. These base wafers then had an ex-situ free layer tunnel junction deposited using the same conditions as run #4 in the second experiment. The coupling fields at various steps in the deposition were measured and are shown below in Table 3.3. The as deposited and post annealed values were taken with a B-H looper while the O-test data represents measurements taken on individual junction R-H loops. To a first order, the coupling fields do not correlate to the AFM surface roughness, however, the in fab B-H data correlates with the O-test data. We have also demonstrated that thinning the free layer thickness to 60A will decrease the coupling field on a standard tunneling wafer from 6.8 to 5.3Oe. In addition, wafers recently deposited using the Comptech sputter system and the sequence from run #4 above have demonstrated coupling fields of less than 5 Oe. The Comptech process uses substrate bias during the deposition process.

Table 3.3. SDT Coupling Data on CMP Copper

	Copper		As Deposited - BH		Post Anneal - BH		O Test - RH	
Wafer	Thickness	AFM Ra	Hc	H coup	Hc	H coup	Hc	H coup
377		SiN	9.5	6.8	4.7	7.4		
233	500	1.8	10.0	7.4	5.8	8.4		
80	1000	4.0	8.9	14.7	7.9	17.9	8.8	17
522	500	6.2	12.1	14.7	6.8	13.7	11.3	9.7
378	500	12.3	10.0	13.7	7.9	13.7		

Figure 3.2 shows the R-H loop of a tunnel junction from a wafer at O-test with a GMR of 26.5%. O-test is the initial electrical test and is conducted after the top electrode has been ion milled down thru the barrier. At this point the free layer is still completely covering the wafer. With the CMP copper underlayer we are able to reduce the field resistance so that accurate measurements of the tunnel junction GMR can be obtained. Testing at O-test will provide faster feedback on material development experiments.

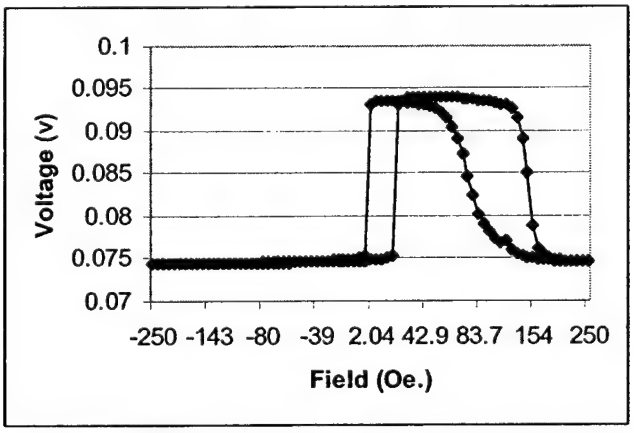

Fig. 3.2. GMR Trace of Tunnel Junction on CMP Copper

The first DOE for tunnel barrier materials development consisted of varying the oxidation time and oxygen flow around the current operating point. We recently struggled with our barrier process only to discover a 0.92 sccm drift in our oxygen m.f.c. caused insufficient oxidization of the deposited Al. As a result, we ordered and installed a 0-10 sccm mass flow controller that will improve our repeatability and accuracy at 3 sccm flow. We also ran the designed experiment outlined in Table 4 which is a simple 2^2 factorial around our current operating point of 2.61 sec. and 3 sccm. The results show that while the current operating point yields similar results as the increased flow conditions, we see significant decrease in GMR as we decrease the flow to 2.5 sccm. Over the range of this experiment we see a 2.2% GMR reduction per sccm flow reduction. As a result of this experiment the operating flow rate of our standard process has been changed to 4 sccm. It should be noted that the first standard wafer was used to set up the ion mill process and consequently was milled for a longer period of time. This causes a decrease in the thickness of the free layer, which increases the field area series resistance and decreases the %GMR. All data from this experiment were taken at Q-test which is after the tunnel junction is completed through the first layer of aluminum interconnect. The resistance area product, RAP, is the product of the resistance of a single junction multiplied by the area of that junction. The results in Table 4 show that the RAP (KOhm-μm^2) increased with increasing oxygen flow that will lead to increased oxidation of the barrier.

Table 3.4. Barrier Oxidation DOE

Time (sec)	Flow (sccm)	% GMR	RAP
2.61	3	9.01	64
2.61	3	20.41	45
2.91	2.5	17.84	48
2.31	2.5	13.82	44
2.91	5	20.99	51
2.31	5	21.63	55

Part 4 – Noise Reduction Circuitry – Dan Reed

The present noise level of a typical SDT sensor as shown in Fig. 4.1 has a 1/f noise spectral density with a level of 4.5nT/√Hz at 1Hz. This 1/f noise is the dominant factor in limiting the device operation at low frequency and must be overcome to obtain the desired noise level of 1pT/√Hz at 1Hz. Although there is hope that improvements in film and junction quality can reduce this 1/f noise, we expect that the sensor measurement circuitry will require an additional noise suppression technique. The approach to suppressing the 1/f noise is to modulate the signal at a higher frequency where the noise is lower, and then demodulate the signal to obtain the low frequency changes in the modulated amplitude. This modulation process will filter out the low frequency noise while still allowing measurement of magnetic fields at low frequency.

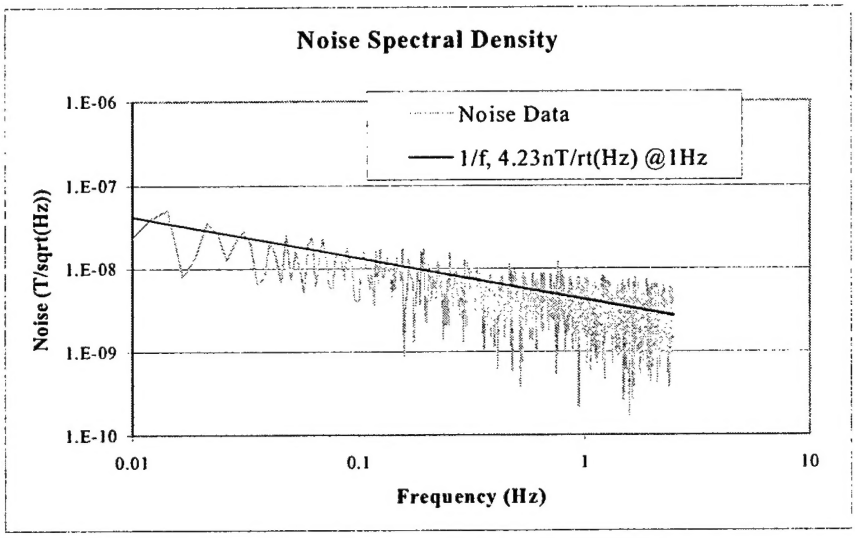

Figure 4.1. The spectral noise density of a typical NVE SDT sensor. The solid line represents a 1/f power spectrum frequency response. The data shows a noise level of 4.24nT/√Hz at 1Hz. This data was taken with no noise suppression circuitry to reduce the 1/f noise.

Bridge Supply Modulation - The first approach used to modulate the sensor signal was to apply a square wave signal to the sensor input and use a lock-in amplifier (LIA) to monitor the sensor response. Fig. 4.2 shows the measurement configuration used to implement this supply modulation. The signal due to the resistance of the SDT bridge will alternate at the chopping frequency, but any slow fluctuation of voltage offset across the tunnel junction will not change at a high chopping frequency. Therefore, only the desired signal and any noise at the chopping frequency will be measured by the LIA. The noise that remains after applying this chopping technique can be measured at the output of the LIA and converted into a noise spectrum similar to that shown in Fig. 4.1. If this chopping technique is successful, then the only noise from the original

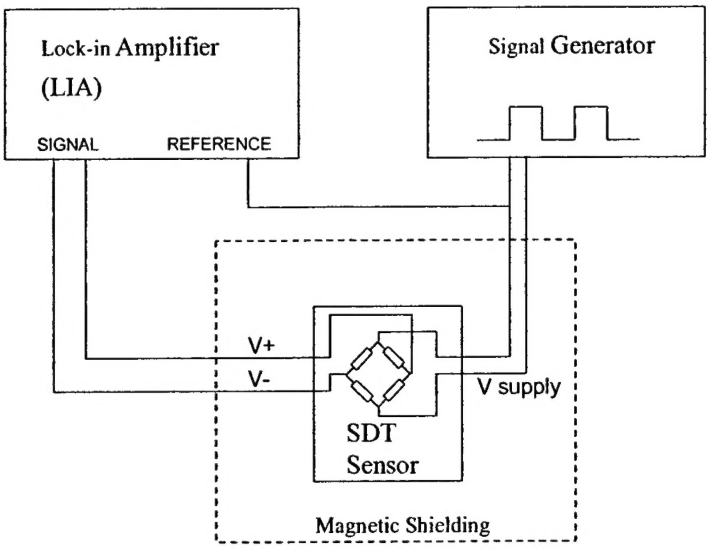

Figure 4.2. Measurement system used to test the approach of modulating the supply voltage to the SDT sensor bridge.

sensor signal that will be measured at the LIA output will be the noise that is very close to the chopping frequency. Because the original sensor signal noise drops off as 1/f, the noise that passes through the chopping should also reduce with higher chopping frequency. However, measurements made with a chopping frequency from 1 Hz to 100kHz showed no change in the noise spectrum measured at the output of the LIA. All noise spectrums had the same 1/f spectrum at the same noise level as the original DC measurements made with no chopping. This result strongly suggests that the noise is not variations in a voltage offset of the sensor, but is instead variations in the bridge resistance.

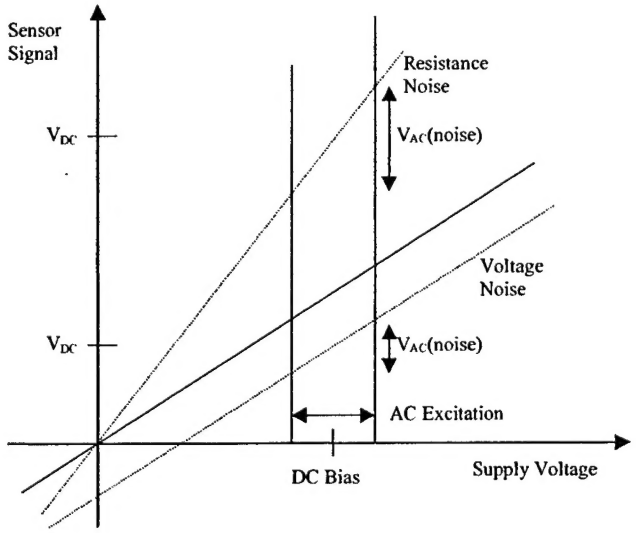

Fig. 4.3. Comparison of voltage noise and resistance noise. By using a DC offset and a small AC excitation signal, both the offset and the slope of the resistance curve can be measured. If the noise source is an offset voltage, then V_{AC} will remain constant while V_{DC} changes. If the noise source is resistance change, then V_{AC} and V_{DC} will both change proportionally.

To confirm that the origin of the sensor noise is a change in resistance of the SDT bridge, I need to verify that the noise signal not only has the same frequency spectrum, but that DC (unchopped) and AC (chopped) signal levels are correlated over time. This time correlation would show that the DC and AC noise are caused by the same source, which could only be caused by resistance changes in the SDT bridge. To measure both the AC and DC noise levels simultaneously, I measured the sensor using a small AC voltage excitation combined with a DC offset voltage as depicted in Fig. 4.3. Fluctuations in a voltage offset would lead only to changes in the measured DC level. Fluctuations in the bridge resistance would cause both the DC and AC signal

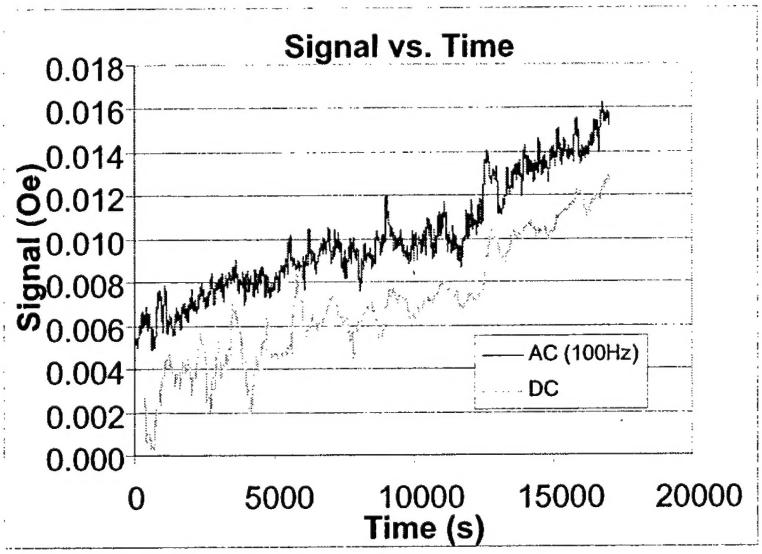

Figure 4.4. Plot of the AC and DC signal levels measured simultaneously versus time. The signal levels are scaled to the same magnetic field signal level, and the average offset value subtracted. Note that the AC signal level is offset slightly to accommodate comparison of the two signals.

levels to change at the same time and by the same proportional amount. By calibrating the AC and DC signals to an applied magnetic field, I can directly compare the two signals as shown in Fig. 4. 4. While the data was measured, the sensor was located in a magnetically shielded chamber with no applied magnetic field. Because the DC measurement has a higher noise level than the AC measurement, the higher frequency noise of the DC signal was digitally filtered using a moving average in the data displayed in Fig. 4.4. However, the low frequency response of the AC and DC signals corresponds identically over time. This confirms that the 1/f noise observed in the sensor is a change in the bridge resistance rather than an additional offset voltage. Noise measurements made with a large permanent magnet used to clamp the magnetic films also show the same noise level, which suggest that the noise is not from the magnetic films. The source of this noise is therefore likely to be fluctuations in the resistance of the tunnel junction.

Conclusions - We have identified that the 1/f noise spectrum observed in the SDT sensors is the result of fluctuations in the resistance of the SDT bridge.

Because a magnetic field signal is also measured by a change in the bridge resistance, it is not possible to use this approach of chopping the bridge source voltage to reduce the sensor noise level. We are therefor pursuing an alternative form of chopping in which the sensitivity of the sensor can be alternatively turned on and off by a chopping signal. This "sensitivity chopping" would allow a direct measure of the sensor resistance with the desired signal and without the signal, providing a means for separating the resistance noise from the desired signal. One approach to providing this "sensitivity chopping" is to send the square wave signal through the sensor bias coil rather than through the sensor bridge. As the bias coil current changes, the sensor's sensitivity to magnetic field also changes.

Future Work - Preliminary measurements using the OC (orthogonal coil) to chop the sensor signal have shown that the magnetic field can be measured with this technique. However, in these measurements the sensor's sensitivity has been substantially reduced so that measurements of the noise have been limited by the noise of the measurement circuits. In order to pursue this measurement technique, it will be necessary to improve the measurement resolution and reduce the noise in the instrumentation used to measure the sensor. Additionally, the signal level will need to be optimized by selecting suitable coil currents for both the high sensitivity and low sensitivity settings. It is still not known whether there will be an increase in magnetic noise associated with applying the chopping OC field. Hysteresis within the magnetic films may lead to some instability that will cause the sensor reading to not be reproducible during each chopping cycle. Improvements in the material quality to lower hysteresis should minimize any noise from this effect. Additional measurements on several sensors will be made to verify the success of this chopping method and to determine the sensor-to-sensor variability of the noise level. Noise spectrum measurements of the sensor signal after chopping will also need to be made over a frequency range up to at least 1kHz to ensure that the method can reliably reduce noise over the frequency range of interest. If this approach is successful in reducing the 1/f noise of the sensor, the circuit used to measure the sensor must be designed to implement the new chopping technique.

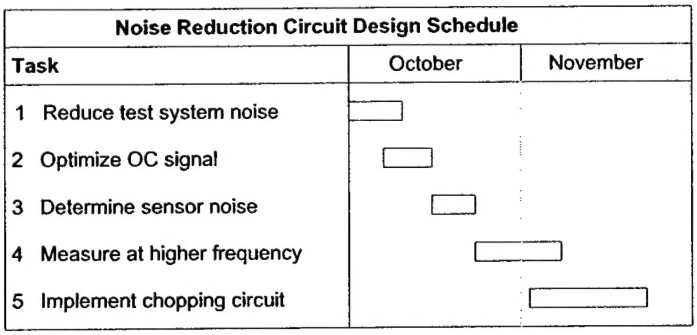

Fig. 4.5. Planned schedule for implementing the othogonal coil chopping technique